Journal of Vibration Engineering & Technologies
https://doi.org/10.1007/s42417-023-01095-0

ORIGINAL PAPER

Site-Specific Amplitude-Distance Laws, Wave Velocities, Damping, and Transfer Functions of the Soil from Hammer Impacts and Application to Railway-Induced Ground Vibration: Similarities and Mid-Frequency Differences

Lutz Auersch[1]

Received: 9 March 2023 / Revised: 20 July 2023 / Accepted: 21 July 2023

Abstract

Purpose The purpose of this article is to check if and how hammer experiments can be applied to the prediction of railway vibration.

Methods The propagation of ground vibrations is theoretically analysed with frequency-wavenumber and simplified methods. Experimental methods are presented which can characterise the site-specific ground vibrations by wave velocities, stiffness and damping. Measurements with hammer and train excitation have been performed at several sites.

Results The one-third octave spectra show the stiffness-dependent amplitudes and the low- and high-frequency filter effects due to the layering and the damping of the soil. Specific train effects, an additional high-frequency filter, the sleeper passage frequency, and an amplified mid-frequency component can be clearly found. The attenuation with distance is analysed in detail where the theoretical exponential and the empirical frequency-dependent power law are considered. Hammer and train excitation show the same site-specific effects which are mainly due to the stronger or weaker damping of the soil. The train attenuation is generally weaker than the hammer attenuation. The attenuation exponent of the power law, which is strongly dependent on the site and the frequency, is reduced for the train vibration by 0.3–0.5 in agreement with the theory. Reasons are discussed for the overall power law and for the dominating mid-frequency component.

Conclusion Therefore, it can be concluded that hammer experiments can well be used for the prediction of train vibrations.

Keywords Hammer impact · Train passage · Layered soil · Attenuation · Filter effects · Randomly heterogeneous soil · Scattering

Introduction

Train-induced vibration can be annoying for inhabitants of nearby buildings. The prediction of these vibrations for a new railway line is based on measurements as far as possible. The vibrations from train excitation can be measured at a different site, but they cannot be directly used for the construction site. The soils at different sites have a strong influence on the amplitudes as well as on the frequency content of the vibration. At the construction site, measurements with artificial sources can be performed [37]. Besides of heavy mass drops [18, 38], small and big vibrators [23, 25, 45], also hammer impacts can be used which are the most simple and practical experiments [5]. Hammer impacts are completely different to the train excitation. The hammer impact is an impulse load and not a quasi-stationary load as for the train passage, it is a fixed point load and not a moving line of many axle loads, and it generates considerably lower amplitudes than the passing train. Therefore it is an important question if and how hammer experiments can be applied to the prediction of railway vibrations.

The prediction and analysis of train-induced vibrations is usually based on the theory of (visco-) elastic wave propagation. The soil (an infinite half-space) can be modelled by finite element systems which need special boundaries, see for example Yang et al. [50], Bayzar and Song [16]. The infinity of the soil is already included in the boundary element method [42], most simply by the Green's functions of the layered soil [6]. The most

✉ Lutz Auersch
lutz.auersch-saworski@bam.de

[1] Federal Institute of Materials Research and Testing, 12200 Berlin, Germany

Published online: 18 August 2023

straight-forward method is the calculation in frequency-wavenumber domain where the differential equations for each soil layer are solved algebraically by matrix methods [5, 26, 31, 47, 49]. The response in the space domain, however, must be calculated by infinite integrals over the wavenumber domain. Some methods use the wavenumber technique along the track and the finite element method across the track, profiting from either the homogeneity or the periodicity along the track [22, 46].

Whatever method is used, the numerical calculations need appropriate parameters which hold for the prediction site. These parameters should be established from experiments at the site. The most important parameter is the wave velocity of the soil which is closely related to the stiffness of the soil. It can be directly evaluated from the arrival times in a seismogram plot. Advanced methods like SASW [39], MASW [10, 41], FK [17], and SPAC [1] have been developed to determine the dispersion in case of a layered soil with a frequency-dependent Rayleigh wave velocity. Layered soil models can be identified from the dispersion curves [36, 42] or from transfer functions [14] Auersch and Said [10].

Experimental investigations on train-induced ground vibration have often been done for a single site or train-track situation to verify the numerical method [2, 24, 30, 42]. Experimental campaigns with more variations to establish certain rules can be found for different train speeds [20], different trains [34], different tracks [36] and from the author, and quite often for mitigation measures, for example in the European project RIVAS [35]. Systematic measurement campaigns with different sites and soils are quite rare [3, 5, 11, 19, 44, 48].

Experimental results for the attenuation of the amplitudes with distance can often be found for the maxima of time histories, for example Auersch and Said [10], Bahrekazemi [15], Kim and Lee [32]. The frequency-dependent attenuation has been studied in Hölzl and Fischer [28] and in Haupt [27]. Theoretical studies about the attenuation can be found in Colombero et al. [18] for the maxima and in Mussat et al. [38] for the frequency-dependent exponential and power law. The attenuation is strongly related to the damping of the soil. Therefore, finite-element calculations with the non-realistic Rayleigh damping, for example Kacimi et al. [21], are not helpful.

The present article is an extended version of the conference contribution [13] where the discussions on the conference motivated some extensions about the experimental methods and the experimental results. The structure of the article is as follows where the additional parts are marked with an asterisk *. The theoretical methods in frequency-wavenumber domain and their approximations are explained in "Theoretical methods"*. Some experimental methods to characterise the soil at the specific site are given in "Experimental methods"*. The measurements are briefly presented in "Measurements of hammer- and train-induced ground vibrations". The measurement results for the attenuation are analysed in "Measurements results for the attenuation" while the measurement results for the transfer functions and spectra follow in "Measurement results for the spectra and transfer functions" where more measurement sites have been added in the present article. Some special (mid-frequency) observations about the attenuation and the spectra of the railway-induced vibrations are discussed in "Discussion of the empirical power law and the special mid-frequency component"* and "Conclusion" provide the conclusions.

Theoretical Methods

Wave Propagation in Frequency-Wavenumber Domain

The wave propagation in a layered soil is solved in frequency-wavenumber (f, k) domain. The compliance $C_{zz}(f, k)$ of the layered soil due to wave excitation is calculated with matrix methods, see Haskell [26], Kausel and Roesset [31], Auersch [5] and Auersch and Said [10]. The response v of the soil to a harmonic point-load excitation F at a distance r is calculated numerically by the wavenumber integral

$$\frac{v}{F}(r,f) = f\int_0^\infty C_{zz}(f,k)J_0(kr)kdk \tag{1}$$

where J_0 is the Bessel function and $C_{zz}(f, k)$ is the vertical compliance of the soil in frequency-wavenumber domain.

Exact and Approximate Wave Velocities (Dispersion)

The wave velocity of the layered soil can be obtained by the maximum of the integrand, the compliance $C_{zz}(f, k)$. The wave velocity depends on the frequency as the layered soil is generally dispersive.

There is a faster alternative to get the approximate dispersion of the soil which has been derived from many examples of exact dispersion results. It is based on the approximated dispersion of a layer of height h_1 on a stiffer half-space with the wave velocities v_{R1} and v_{R2}

$$v_R(f) = v_{R1} + (v_{R2} - v_{R1})0.5\left(1 + \cos\frac{\pi}{2}\frac{f}{f_1}\right) \text{with} f_1 = \frac{v_{S1}}{3h_1} \tag{2}$$

which is extended to a multi-layered situation. A correction for each layer is added to the wave speed v_{R1} of the top layer

$$v_R(f) = v_{R1} + \sum_{i=1}^{n-1}(v_{Ri+1} - v_{Ri})0.5\left(1 + cos\frac{\pi}{2}\frac{f}{f_i}\right) \text{with} f_i = \frac{v_{Si}}{3h_i} \tag{3}$$

h_i is the depth where the layer i ends. For very low frequencies, the wave speed of the underlying half-space can be reached.

Exact and Approximate Point-Load Solutions for Homogeneous and Layered Soils

The infinite wavenumber integral (1) can be approximated by a special method, the dispersal soil method [9], which is based on the two asymptotes for the transfer function of the homogeneous soil [33]

$$\frac{v}{F}(r,f) = \frac{f(1-\nu)}{Gr}\exp(-2\pi D r^*)$$
$$\begin{cases} 1 & \text{for } r^* \le {r_0}^* \\ \sqrt{r^*/{r_0}^*} & \text{for } r^* > {r_0}^* \end{cases} \text{ with } r^* = \frac{fr}{v_S} \text{ and } {r_0}^* = 0.43 \quad (4)$$

with G the shear modulus, ν the Poisson ratio, D the damping, and v_S the shear wave velocity of the soil. The asymptotes (4) consist of a power law

$$A \sim r^{-1} \text{ for the nearfield } \left(r * < r_0 *\right) \quad (5)$$

or

$$A \sim r^{-0.5} \text{ for the farfield } \left(r * < r_0 *\right) \quad (6)$$

and of an exponential factor

$$A \sim \exp(-2\pi D r *) \quad (7)$$

due to the material damping of the soil. In case of a layered soil, the same asymptotes of a homogeneous soil have been used but with a frequency-dependent stiffness and wave velocity according to the dispersion relation (2) and (3). The asymptotic expressions for the dispersion and the transfer function yield a fast prediction in a good quality by avoiding lengthy calculations in wavenumber domain, see the comparison in [9]. The fast approximations are necessary when many point loads have to be calculated for a train load whereas the exact integral (1) is feasible for a single point load.

To compare the measured results with theory, the transfer functions for some typical soil situations are calculated by Eq. (1) and the resulting one-third of octave spectra are shown in Fig. 1 for source-receiver distances between 4 and 64 m. The spectra are increasing with frequency, first with $v \sim f$ at low frequencies, and with $v \sim f^{1.5}$ in a mid-frequency range. At high frequency, the exponential function of the damping is dominating and the curves start to decrease. For soft soils (Fig. 1a), high damping, or long distances, the exponential damping effect is strong whereas the power laws of the geometric attenuation is more dominant for stiff soils (Fig. 1b). In case of a layered soil (Fig. 1c) the transfer function follows that of a homogeneous half-space with

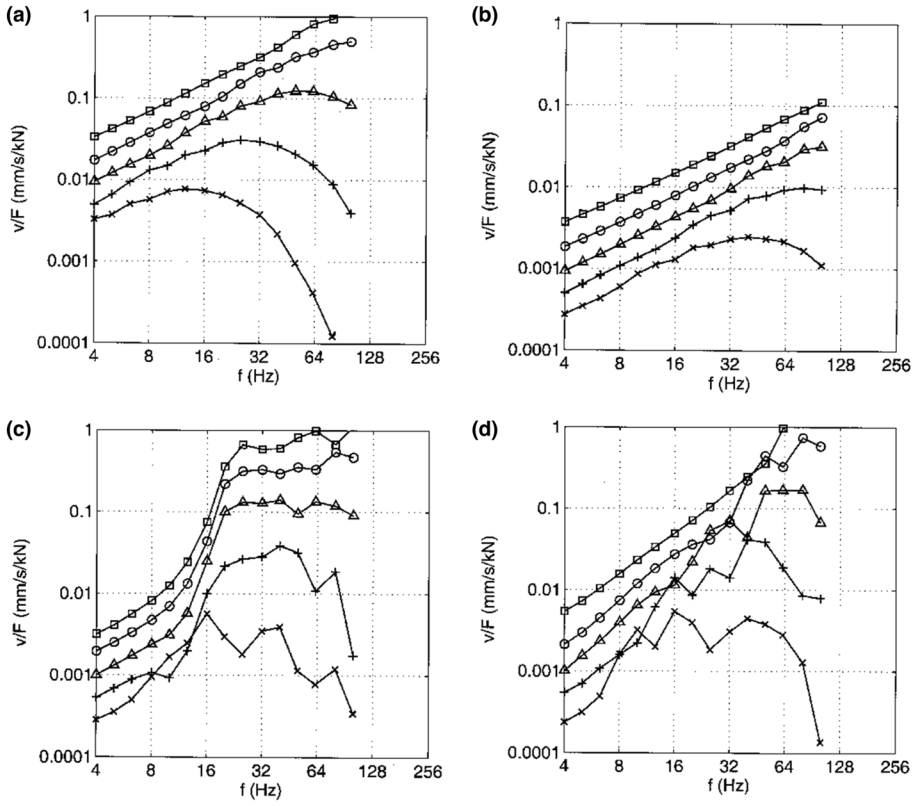

Fig. 1 Transfer functions for different soils, homogeneous soil of **a** $v_S = 100$ m/s and **b** $v_S = 300$ m/s, **c** layer on a half-space, $v_{S1} = 100$ m/s, $v_{S2} = 300$ m/s, $h = 2$ m, **d** soil with increasing stiffness, $v_S = 100$–300 m/s, distances square 4, circle 8, triangle 16, plus 32, cross 64 m from the source, damping $D = 2.5\%$

the higher stiffness of the underlying soil at low frequencies whereas it follows the homogeneous transfer function of the softer upper layer at high frequencies. The transition from the stiff to the soft behaviour occurs around the layer frequency f_1 where a strong increase can be observed. A moderate resonance amplification at the layer frequency is possible. If the stiffness of the soil increases continuously with depth (Fig. 1d), there is a continuous softening of the soil with frequency and the spectra increase as $v \sim f^p$ with $p > 1$ stronger than for a homogeneous soil before the damping starts to dominate.

Train-Load Solution from the Superposition of Point Loads

The response for a train load is calculated as the superposition of point loads, one for each wheelset along the train length (coordinate y), see also [40]

$$v(x,f) = \sqrt{\sum_{j=1}^{n} H_P{}^2(\sqrt{x^2 + y_j{}^2}, f)F(f)} \tag{8}$$

The distribution of the axle load across the track width (coordinate x) is incorporated by the factor

$$\frac{v_a}{v_0} = \frac{\left|\int_{-a}^{+a} e^{j\omega x/v_S} dx\right|}{2a} = \frac{|\sin \omega a/v_S|}{\omega a/v_S} \le \frac{1}{\omega a/v_S} \text{ for} \frac{\omega a}{v_S} > \frac{\pi}{2} \tag{9}$$

which yields an additional filter (a reduction) for the high frequencies $\omega = 2\pi f$. The response of a standard train with a constant load spectrum $F(f) = 1$ kN is shown for a soil with $v_S = 200$ m/s in Fig. 2b in comparison with the transfer function of a point load (Fig. 2a). Because of the many loads along the train, the response is stronger at long distances and the curves are closer together. Because of the distribution across the track, the high frequencies are reduced stronger than for the point load. Therefore, the dominance of the mid frequencies is even more pronounced for the train load than for a point load (a hammer excitation).

Attenuation of Amplitudes with Distance

The response of the soil in Figs. 1 and 2 can be evaluated for the amplitude-distance law (the attenuation with distance). These attenuation curves will be plotted for 10, 20, 40 and 80 Hz in double logarithmic scales in "Evaluation of the attenuation by the empirical power law". The power law results in a straight line, the exponential function yields a curve bending down for higher distances.

The response to a long (passenger) train has a weaker attenuation than the point load. This means that the attenuation curves are somewhat less steep. If the train is short, for example a tram or other urban traffic, the attenuation is between the stronger point-load and the weaker long-train attenuation. The point load for a softer soil or with a higher damping has a strong attenuation for all distances at least with $A \sim r^{-1}$. The weaker attenuation with $A \sim r^{-0.5}$, which holds for an elastic Rayleigh wave, can only be found for stiff soils and little damping. The attenuation clearly depends on the soil for the specific site. More detailed results for short trains and for longer distances (100 m and more) and an analytic expression can be found in Auersch [4]. There it is also shown that the attenuation for a train on a damped soil can be found by multiplying the exponential damping factor (7) with the response for the elastic (undamped) soil.

Experimental Methods

The response of the soil to the hammer, drop weight, shaker or train excitation is measured with a line of velocity sensors (geophones) fixed to the soil by spikes. The measurement points for the amplitude are placed in a logarithmic scale such as 3, 5, 10, 20, 30, 50 m or 4,

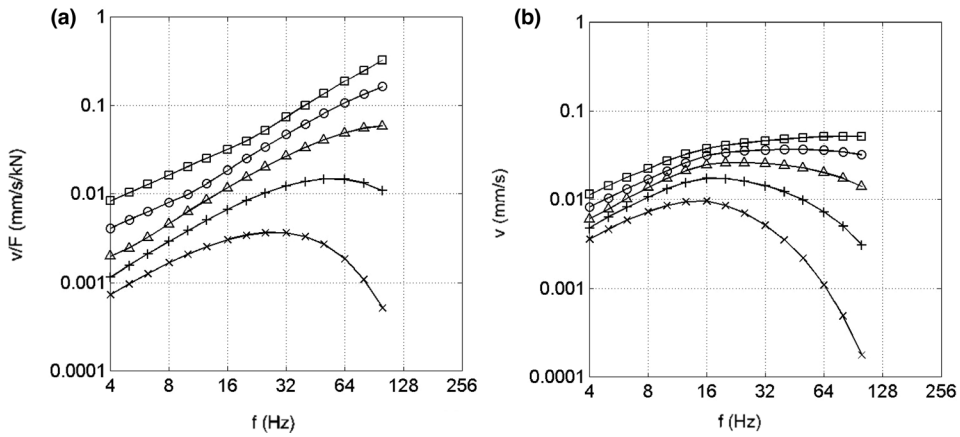

Fig. 2 Transfer functions for a point load (**a**) and for a standard train load (**b**), homogeneous soil of $v_S = 200$ m/s, $D = 2.5\%$

8, 16, 32, 64 m. The wave velocities are measured with equidistant sensors (for example at every 2 m) at a distance of typically 15–30 m from the source which is on the soil surface in most cases. The two measurement lines are usually combined in one measurement line perpendicular to the railway track, but the wave-velocity line is sometimes placed parallel to the track due to space or access limitations. The analog signals are converted to digital data in a measuring system with 72 channels of sample-and-hold amplifiers, programmable analog filters, and a sampling rate of 2 kHz has been used.

Wave Velocities from Simple and Advanced Methods

The wave velocities are evaluated by different methods. The most simple method is the seismogram plot which works well if the soil is almost homogeneous (Fig. 3). The evaluation of the onsets of the waves could be assisted by the

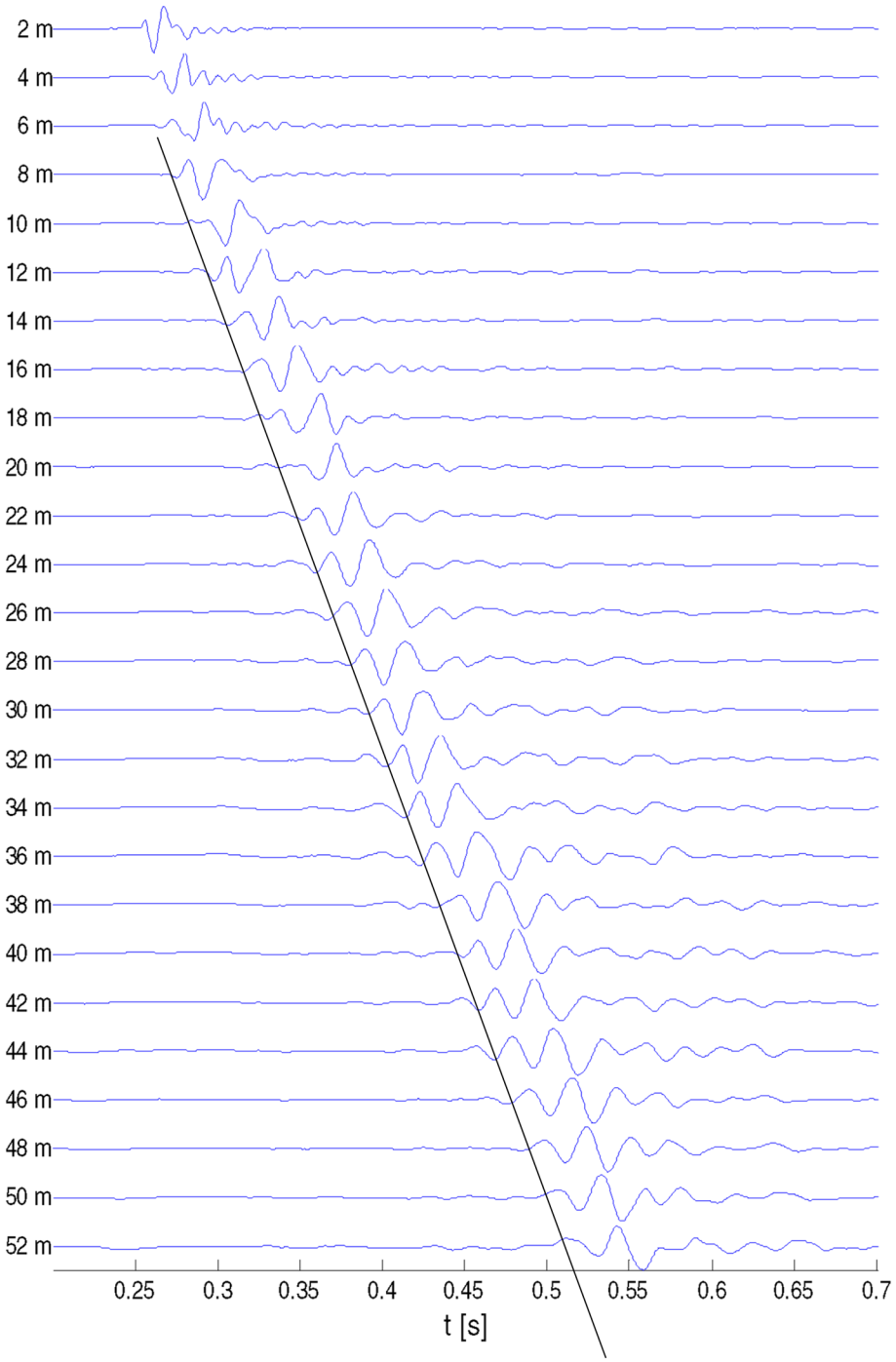

Fig. 3 Wave velocity of a homogeneous soil from a seismogram plot

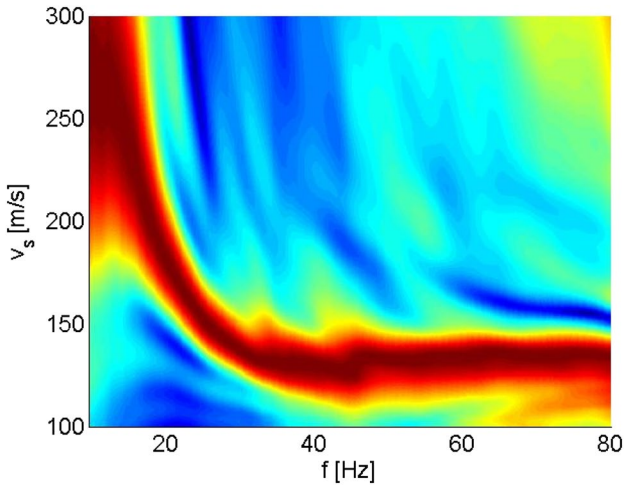

Fig. 4 Wave velocity of a layered soil from a frequency-wavenumber transform

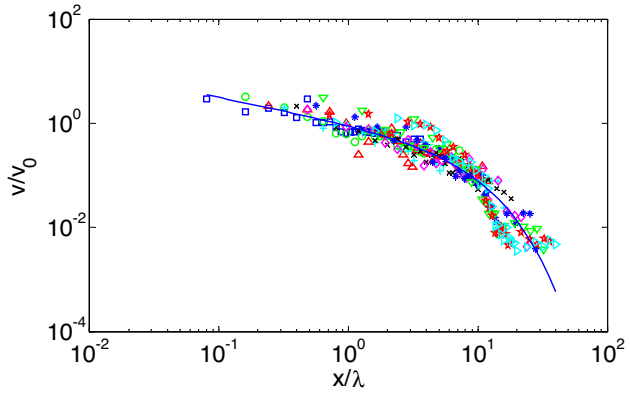

Fig. 5 Damping from a normalised amplitude-distance plot

correlation maxima between two adjacent sensors. Advanced procedures (SASW, MASW, FK, SPAC) using frequency or wavenumber spectra can be applied to establish the dispersion of a layered soil (Auersch 2015). An example is given in Fig. 4. The normal layering of the soil, where the stiffness is increasing with depth, results in a dispersion with a wave velocity which is decreasing with frequency.

Damping from a Normalised Amplitude-Distance Law

The material damping D of the soil is measured by the attenuation of the amplitudes A. The attenuation of different frequencies is considered at the same time. A unique amplitude-distance relation can be found in (Fig. 5) if it is written as

$$A = Cr*^{-q}\exp(-2\pi Dr*) \tag{10}$$

with a constant C and a normalised distance $r^*=r/\lambda$, the distance r related to the wavelength λ. Such an equation holds for every frequency and for every distance measured. If the logarithm of these equations is taken, a set of linear equations of the unknown parameters q, D and $\ln C$

$$\ln A = \ln C - q \ln r* - 2\pi Dr* \tag{11}$$

is obtained. The best approximation of these equations is calculated giving the geometrical attenuation q, the material damping D, and the $\ln C$.

The Eqs. (10,11) can be simplified if the power q is prescribed, for example as $q=0.5$ for the Rayleigh wave. Moreover, the procedures could also be followed for each frequency and a frequency-dependent damping could be established. But this is practically not relevant as the damping is usually only interesting for the high frequencies. The use of the logarithmic measurement axis is highly recommended as the damping effect is found at far distances. The shorter equidistant measurement line would be not so significant.

Transfer Functions and Train-Induced Ground Vibrations

The response $v(f)$ of the soil can be transformed to the transfer (admittance) function $v/F(f)$ if the exciting (hammer or shaker) force $F(f)$ has been measured. The transfer functions of all near- and far-field measurement points are plotted as one-third of octave spectra in a single plot in the same way as the train-induced ground vibrations.

Identification of a Soil Model

The soil model for a specific site (these are essentially the wave velocities and the thicknesses of the soil layers) can be obtained either from the dispersion or from the set of transfer functions. For a certain set of parameters, the dispersion or the transfer functions are calculated and compared with the measured dispersion or transfer functions. This calculation must be repeated for many parameter sets so that the best fit (the minimum of the error) can be found in a grid search. To get the result in an acceptable calculation time it is advantageous to use the approximate solutions of "Exact and approximate wave velocities (dispersion)" and "Exact and approximate point-load solutions for homogeneous and layered soils" and to focus on a significant parameter set, for example of a 2-layer soil model. 2-layer soil models have been identified for the Swiss measurement sites by approximating the transfer functions and are given in the captions of Figs. 7 and 8.

The soil model is used to make predictions on the base of the corresponding calculated transfer functions. The measured transfer functions could be used directly, but it is necessary to make some interpolations and extrapolations. It should be noted that the response to hammer impacts has usually low amplitudes at low frequencies so that there is some uncertainty for the transfer functions. The prediction of train-induced vibrations is most important in the mid-frequency range and the uncertainty at low frequencies is, as well as the simplified soil model, acceptable.

Evaluation of the Attenuation by the Empirical Power Law

In the literature (for example [3, 18, 28, 32, 38]) an empirical attenuation law can be found which is a power law $A \sim r^{-q}$ with a site- and source-specific power q. These attenuation laws are presented in Fig. 6b with the same overall attenuation as the theoretical exponential law in Fig. 6a. The power laws are straight lines in the double logarithmic presentation which have higher exponents and have a steeper descent for higher frequencies. The weaker attenuation for the superposition of the train loads in Fig. 6c, d can be directly recognised by the lower exponents which are written on the right of the curves. The relative amplitudes of the octaves around 10 (12), 20 (16–25), 40 (32–50), and 80 (64–100) Hz are plotted in the double logarithmic attenuation Figs. 7 and 8 evaluated for the overall attenuation power q.

Measurements of Hammer- and Train-Induced Ground Vibrations

The Federal Institute of Material Research and Testing has performed measurements of train-induced ground vibrations at many different sites. Hammer impacts and wave velocity measurements have been applied whenever possible. The evaluation of the dispersion with advanced methods has been done for the later measurements, namely for two series of measurements in Switzerland. From dispersion and transfer function measurements layered soil models have been identified. For the other measurements at least the dominating wave velocity and damping have been established. The measurement results of 12 sites are presented in Fig. 7 as amplitude-distance laws and in Fig. 8 as spectra for train and hammer excitations.

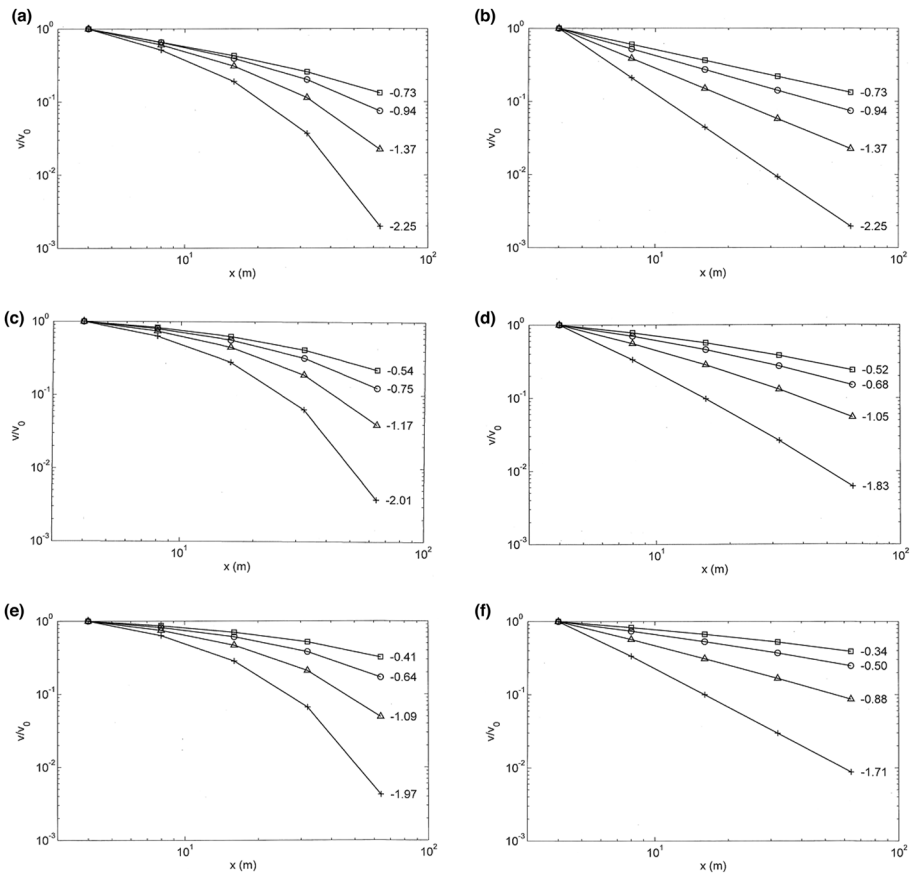

Fig. 6 Calculated attenuation laws for a point load (**a**, **b**), for a short train (**c**, **d**) and for a long train (**e**, **f**), theoretical law $A \sim r^{-0.5}\exp(-D\omega r/v_R)$ (**a**, **c**, **e**) and empirical law $A \sim r^{-q}$ (**b**, **d**, **f**)

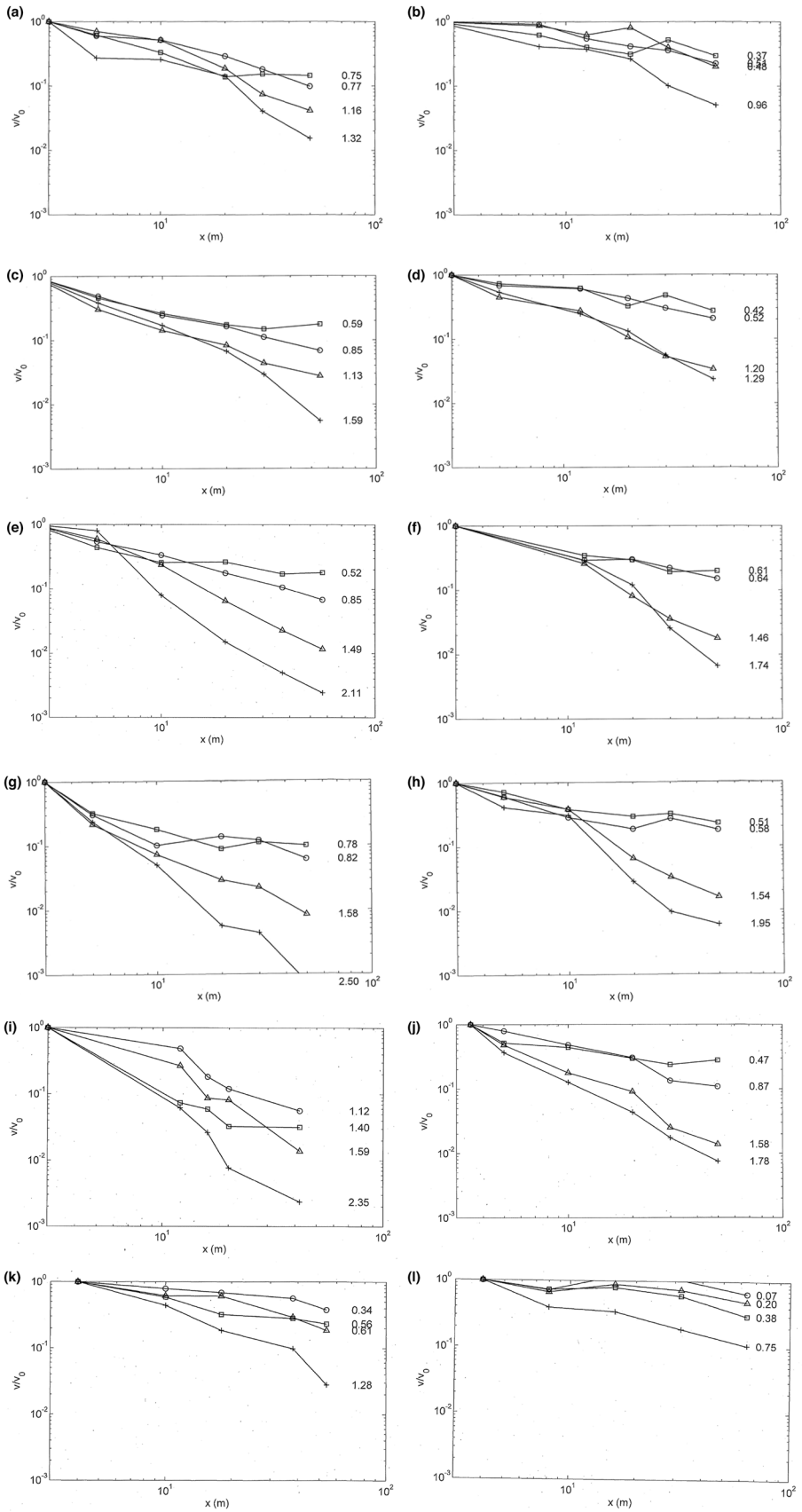

Fig. 7 Measured attenuation laws from hammer excitation (left) and train excitation (right) at **a**, **b** Site W (v_S = 270, 1000 m/s, h = 10 m), train speed v_T = 125 km/h, **c**, **d** Site H (v_S = 225 m/s, v_T = 130 km/h), **e**, **f** Site H* (v_S = 225 m/s, v_T = 130 km/h), **g**, **h** Site N (v_S = 120–200 m/s, v_T = 130 km/h), **i**, **j** Site S (v_S = 125, 250, 750 m/s, h = 2, 4 m, v_T = 100 km/h), **k**, **l** Site G (v_S = 170 m/s, v_T = 250 km/h), **m**, **n** Site G* (v_S = 200 m/s, v_T = 250 km/h), **o**, **p** Site A (v_S = 125, 250 m/s, h = 4 m, v_T = 160 km/h), **q**, **r** Site D (v_S = 150, 300 m/s, h = 2.5 m, v_T = 130 km/h), **s**, **t** Site O (v_S = 150, 350 m/s, h = 1 m, v_T = 80 km/h), **u**, **v** Site X (v_S = 125, 350 m/s, h = 2.5 m, v_T = 160 km/h), **w**, **x** Site C (v_S = 150, 450 m/s, h = 1.5 m, v_T = 160 km/h)

Fig. 7 (continued)

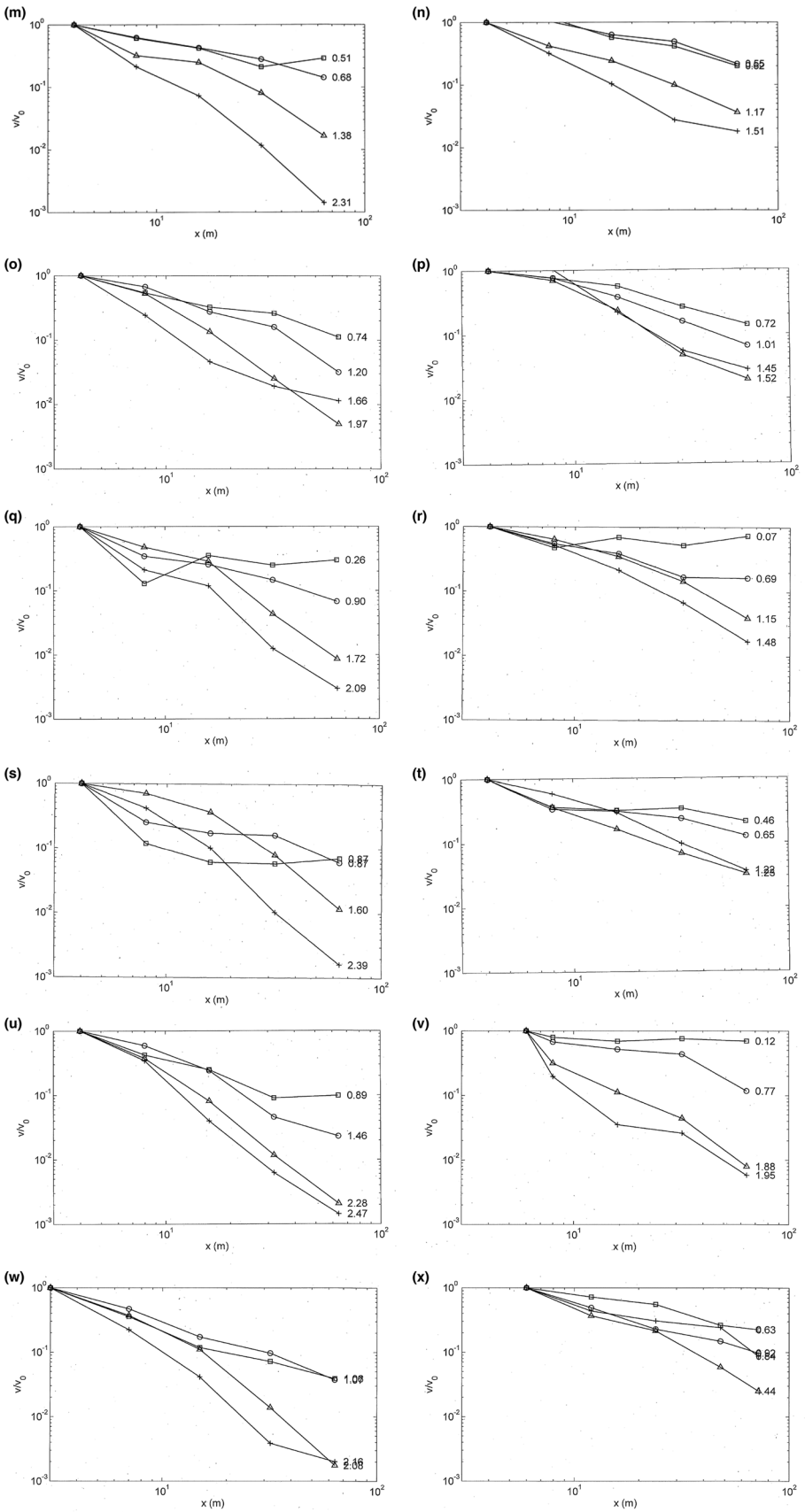

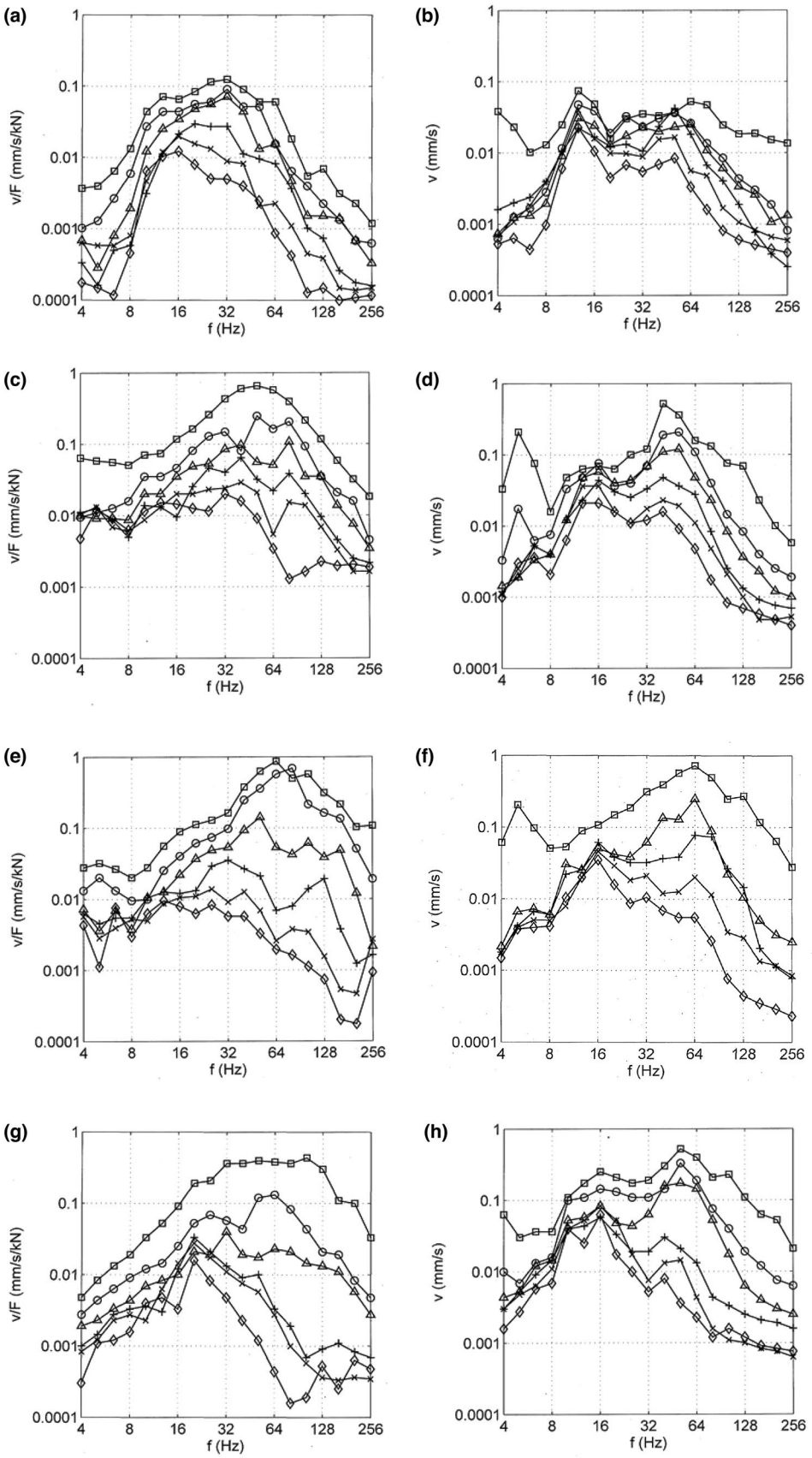

Fig. 8 Measured spectra from hammer excitation (left) and train excitation (right) at **a**, **b** Site W ($v_S = 270$, 1000 m/s, $h = 10$ m), train speed $v_T = 125$ km/h, **c**, **d** Site H ($v_S = 225$ m/s, $v_T = 160$ km/h), **e**, **f** Site H* ($v_S = 225$ m/s, $v_T = 160$ km/h), **g**, **h** Site N ($v_S = 120$–200 m/s, $v_T = 130$ km/h), **i**, **j** Site S ($v_S = 125$, 250, 750 m/s, $h = 2$, 4 m, $v_T = 100$ km/h), **k**, **l** Site G ($v_S = 170$ m/s, $v_T = 250$ km/h), **m**, **n** Site G* ($v_S = 200$ m/s, $v_T = 250$ km/h), **o**, **p** Site A ($v_S = 125$, 250 m/s, $h = 4$ m, $v_T = 160$ km/h), **q**, **r** Site D ($v_S = 150$, 300 m/s, $h = 2.5$ m, $v_T = 130$ km/h), **s**, **t** Site O ($v_S = 150$, 350 m/s, $h = 1$ m, $v_T = 80$ km/h), **u**, **v** Site X ($v_S = 125$, 350 m/s, $h = 2.5$ m, $v_T = 160$ km/h), **w**, **x** Site C ($v_S = 150$, 450 m/s, $h = 1.5$ m, $v_T = 160$ km/h, at distances $r \approx$ square 3, circle 5, triangle 10, plus 20, cross 30, diamond 50 m (**a**–**j**) and $r \approx$ square 4, circle 8, triangle 16, plus 32, cross 64 m (**k**–**x**)

Fig. 8 (continued)

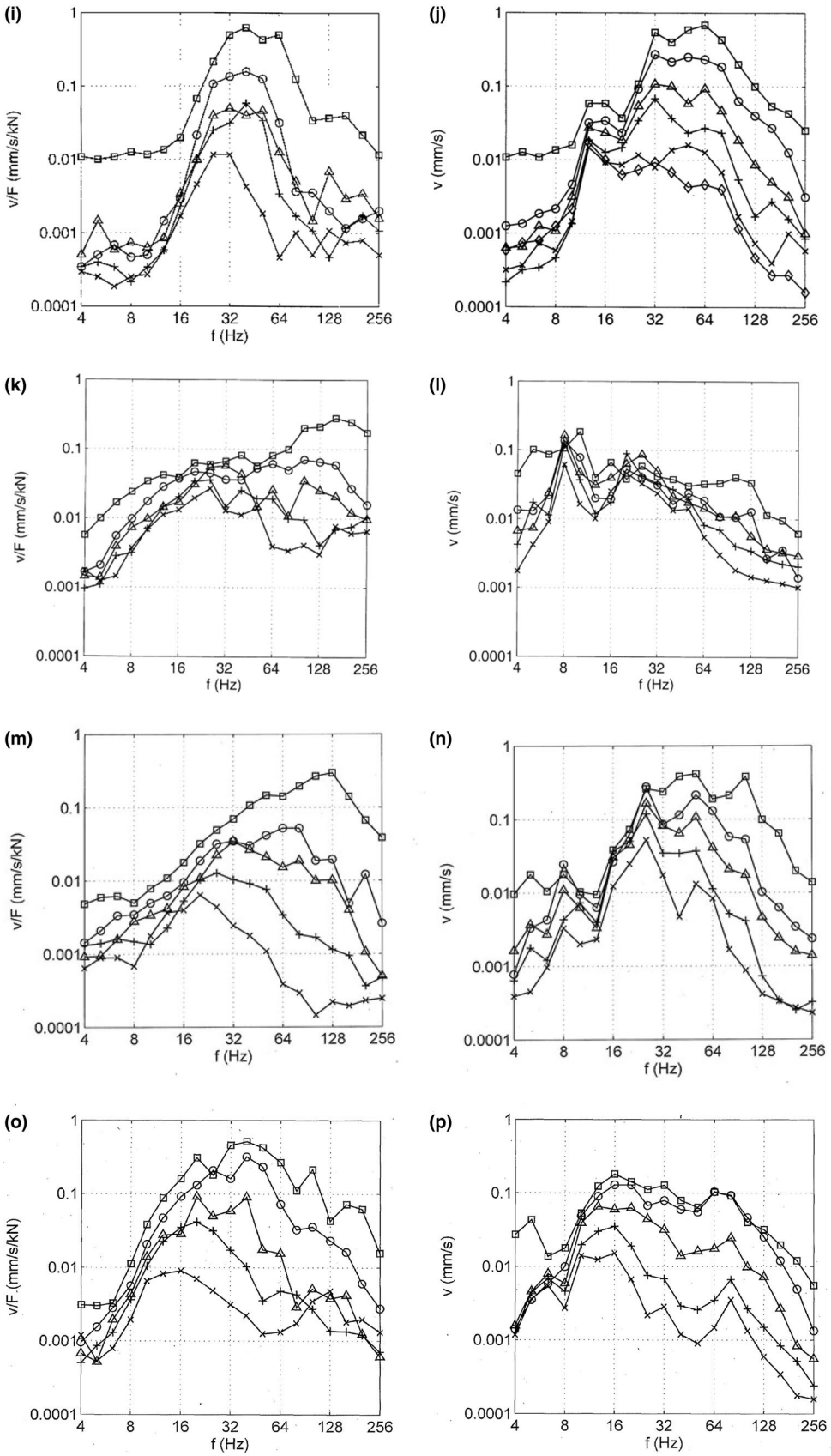

Fig. 8 (continued)

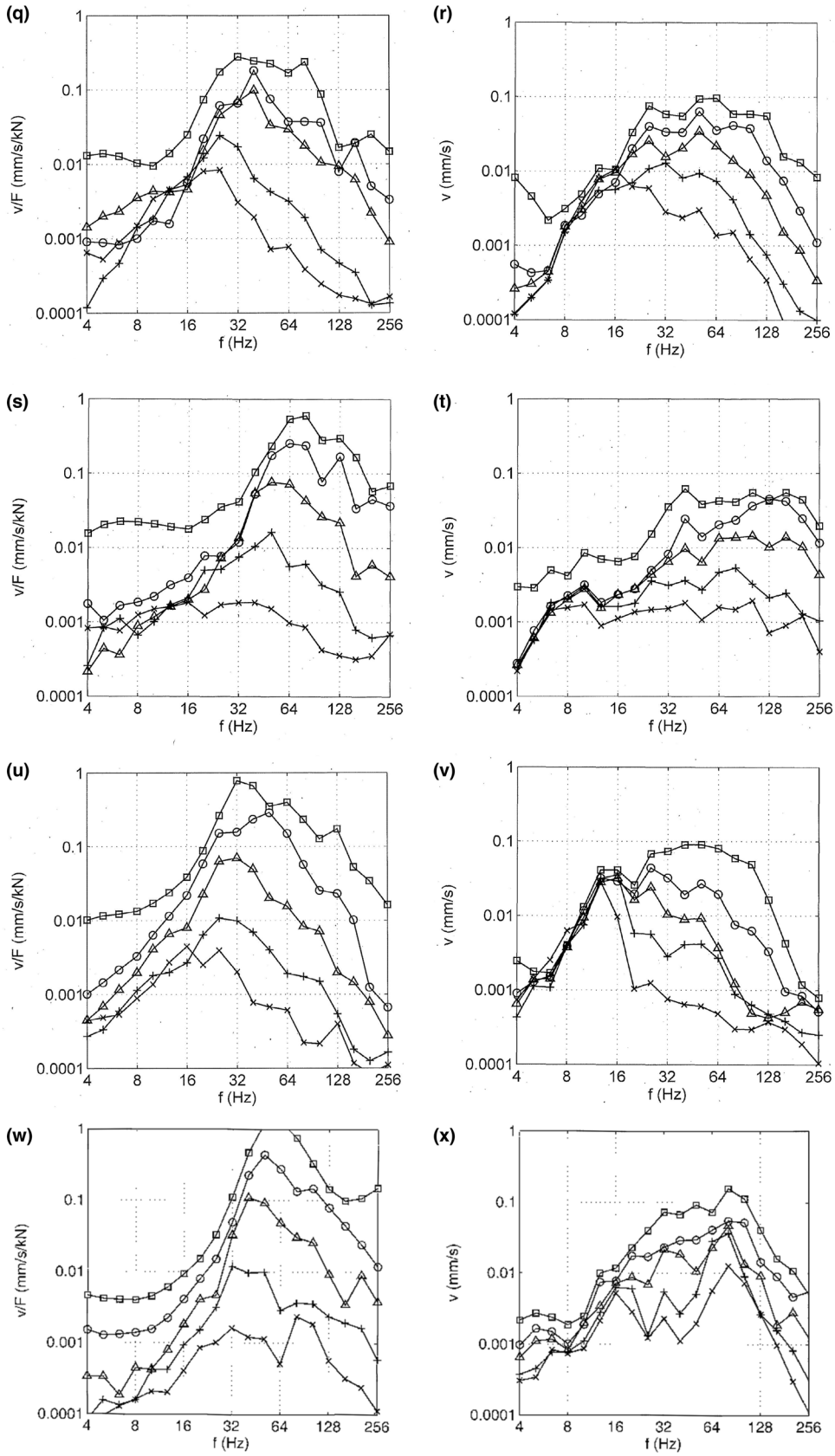

Measurements Results for the Attenuation

All amplitude distance-laws in Fig. 7 show the strong attenuation for higher frequencies (the octaves of 40 and 80 Hz) which is due to the damping of the soil. The lower frequencies of 10 and 20 Hz have a weak attenuation and the curves are almost straight lines indicating a power law $v \sim r^{-q}$. The power q for these frequencies is usually in the range from 0.4 to 0.6 for train excitation and between 0.5 and 0.9 for hammer excitation. The attenuation curves for the high frequencies have different shapes. In Fig. 6a, c, f, m, o, s, w the high-frequency curves follow the exponential function from the theory of a homogeneous half-space where the attenuation is increasing with distance. This characteristic cannot be found for the other high-frequency curves. They are rather straight lines and that means a power-law attenuation. The attenuation powers q are between 1.0 and 2.5 for hammer impacts and between 0.5 and 2.0 for trains, much higher than for the low frequencies. Similar attenuation exponents can be attributed to the more exponential amplitude-distance laws as a rough approximation. The wide ranges of attenuation exponents indicates that the attenuation varies considerably from site to site.

For the situation where hammer impacts are used to predict the attenuation of train-induced ground vibrations, it can be followed from these figures that the site-specific attenuation is very similar for train and hammer excitation. If there is a strong attenuation due to the strong damping of the soil this can be found in both measurements, see the examples in Fig. 7e + f, g + h, i + j, q + r, u + v. The same similarity of hammer- and train-induced vibrations holds for the weak damping at sites W, H, and G in Fig. 7a + b, c + d, k + l. Site G (Fig. 7k + l) has the weakest attenuation of all sites. Moreover, there is almost no attenuation of the 20 Hz octave for the high-speed train (Fig. 7l, n). The same weak attenuation is observed for site D (Fig. 7r) and site X (Fig. 7v) at the 10 Hz octave for normal train speeds. Moreover, a clear difference in the attenuation between the low frequencies (10 and 20 Hz) and the high frequencies (40 and 80 Hz) can be observed in Fig. 7d, f, h, j. All these effects of reduced attenuation seem to be related to a special train-induced mid-frequency component (see also "Measurement results for the spectra and transfer functions" and "Discussion of the empirical power law and the special mid-frequency component").

The attenuation of hammer induced vibrations are always stronger than the attenuation from train measurements. The difference between the two attenuation exponents has been evaluated for each site and each octave. It is increasing with frequency and the average for all sites lies between $\Delta q = 0.2$ and 0.6 which is close to the theoretical values of $\Delta q = 0.3$ and 0.5.

Measurement Results for the Spectra and Transfer Functions

Figure 8 shows the spectra for the hammer and the train excitation for the 12 measurements sites in Germany and Switzerland. The spectra are clearly site-specific. Moreover, the same characteristics of a special site can be found in the hammer as well as in the train spectra. The similarity of the transfer functions from hammer excitation and the response to the passing train is due to the rather smooth and constant force spectra of the dynamic train loads which are also close to the value 1 kN per axle and one third of octave [8].

The following site-specific characteristics can be observed. At first, the sites with softer soils (Fig. 8g + h, k + l, o, p + p, u + v) have generally higher amplitudes, mainly at the low and mid-frequency range. At higher frequencies, the spectra and especially the train-induced spectra turn to horizontal curves whereas the spectra continue to increase for the stiff sites in Figs. 8q + r, s + t. The behaviour at high frequency indicates if there is a weak or a strong damping. The curves for sites with low damping (Fig. 8a + b, c + d, k + l) stay closer together whereas there is a considerable spread of the curves for high damping (Fig. 8e + f, g + h, m + n, u + v). The low-frequency behaviour of the spectra gives some information on the layering of the soil. From the weak low-frequency increase of the spectra, it can be concluded that the sites H, H*, G, G* (Fig. 8c–f, k–n) are nearly homogeneous soils. The site N (Fig. 8g + h) has soils with a continuously increasing stiffness and a continuously stronger increase of amplitudes with frequency. The sites W, S, D, O, C (Fig. 8a, I, q, s, w) are clearly layered soils with a strong increase around the layer frequency. The layered sites differ in their layer frequency which is at 12 Hz for site W (Fig. 8a), at 16 Hz for site A (Fig. 8o), at 20–32 Hz for site D (Fig. 8q), at 25 Hz for site X (Fig. 8u), at 32 Hz for site S (Fig. 8i), at 50 Hz for site C (Fig. 8w), and at 64 Hz at site O (Fig. 8s), where a high layer frequency generally means a thinner top layer. Because of the low-frequency characteristics of the layering and the high-frequency filter of the damping, a site-specific mid-frequency range with maximum amplitudes is dominating, especially in the far field.

Some special frequencies can be observed in the train-induced spectra. The high-frequency peaks at 40 Hz for 80 km/h (Fig. 8t) to 100 Hz for 250 km/h (Fig. 8l, n) are generated by the sleeper distance. A specific train-induced component can be found at 10 to 16 Hz for normal speeds (Fig. 8b, d, h, j, v) and at around 25 Hz for 250 km/h (Fig. 8l, n). There are three thirds of octave where the attenuation is weak (the curves come close together) and the amplitudes are raised. Such a mid-frequency effect can be observed at almost all measurement sites and it is assumed that this is

due to the scattering of the axle impulses by a randomly varying soil stiffness.

Some more specialties have been observed for urban traffic. The short tram in Fig. 9a shows a rather strong attenuation at high frequencies but also at low frequencies in agreement with theory. For a metro train close to the surface (Fig. 9b), a weak attenuation can be seen for low frequencies which might be a consequence of the wider distribution of each axle load due to the stiff tunnel structure.

Discussion of the Empirical Power Law and the Special Mid-Frequency Component

Experiments with hammer impacts confirm the exponential attenuation law when all frequencies are considered in the evaluation scheme for the damping ratio, see the continuous line in Fig. 5. The (normalised) amplitudes for all measurement points (normalised distances) and of a single frequency are plotted with a specific marker in a specific colour. These results of a single frequency resemble rather a pure power-law attenuation than an exponential law. The power law could have the following reasons.

The layering of the soil weakens the exponential law of the homogeneous soil at high frequencies when the less damped deeper soils become dominant over the strongly damped top layer, see Fig. 1c compared to Fig. 1a.

A broad-band constant spectrum A_0 at a near-field point yields an additional attenuation exponent of $\Delta q = 0.5$ instead of the different exponential laws for each frequency (Fig. 10)

$$\sqrt{M(v^2)} \sim \sqrt{\int_0^\infty \frac{{A_0}^2}{r}\left(exp\left(-\frac{\omega D}{v_R}r\right)\right)^2 d\omega} = \frac{A_0}{\sqrt{r}}\sqrt{\frac{v_R}{2Dr}} \sim r^{-1.0} \tag{12}$$

This effect could also be expected for a single frequency if there is an interference of different wave modes of the layered soil.

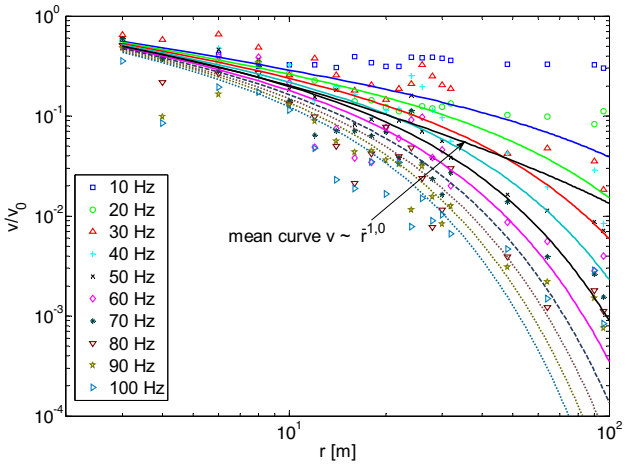

Fig. 10 Attenuation laws for measured frequency components (date points) and from calculated broad-band excitation (lines), sum of exponential laws yield a power law (black line)

The material damping of the soil is non-linear in general. The smaller the amplitudes in the far field the weaker is the damping and the corresponding attenuation. Therefore, the exponential attenuation of the constant damping would turn into a more straight-line (power-law) attenuation.

Waves are scattered at the heterogeneities of a real soil and a part of the wave energy disappears in the depth of the soil. The scattering results in a similar exponential amplitude-distance relation $A \sim \exp(-D_S \omega r / v_R)$ as the material damping [43]. The attenuation can be linearly increasing with frequency similar to the hysteretic material damping, but also stronger dependencies on the frequency are possible [7].

The moving static train loads result in the low-frequency quasi-static response of the soil which has a strong attenuation ($f < 10$ Hz in Fig. 11b), see [9]. A corresponding maximum at 4 or 5 Hz can be seen at the nearest measurement point in Fig. 8b, d, f, h, p, r. This quasi-static response could be strongly amplified for a train running with Rayleigh wave speed, but this effect (like a sonic boom) cannot occur in a heterogeneous soil [11]. On the other hand, the variation of

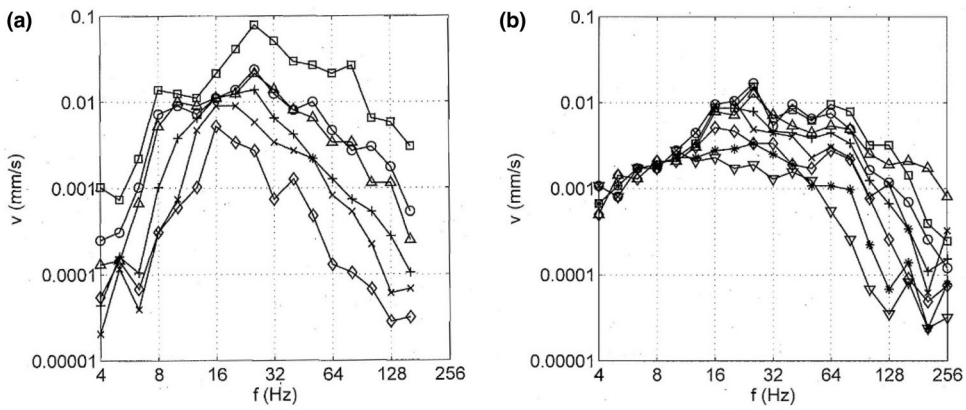

Fig. 9 Measured spectra from urban trains, **a** tram at site K, r = square 6, circle10, triangle 14, plus 20, cross 35, diamond 55 m, **b** Metro at Site B, r = square 8, circle 12, triangle 16, plus 24, cross 32,diamond 48,asterisk 96, inverted triangle 128 m

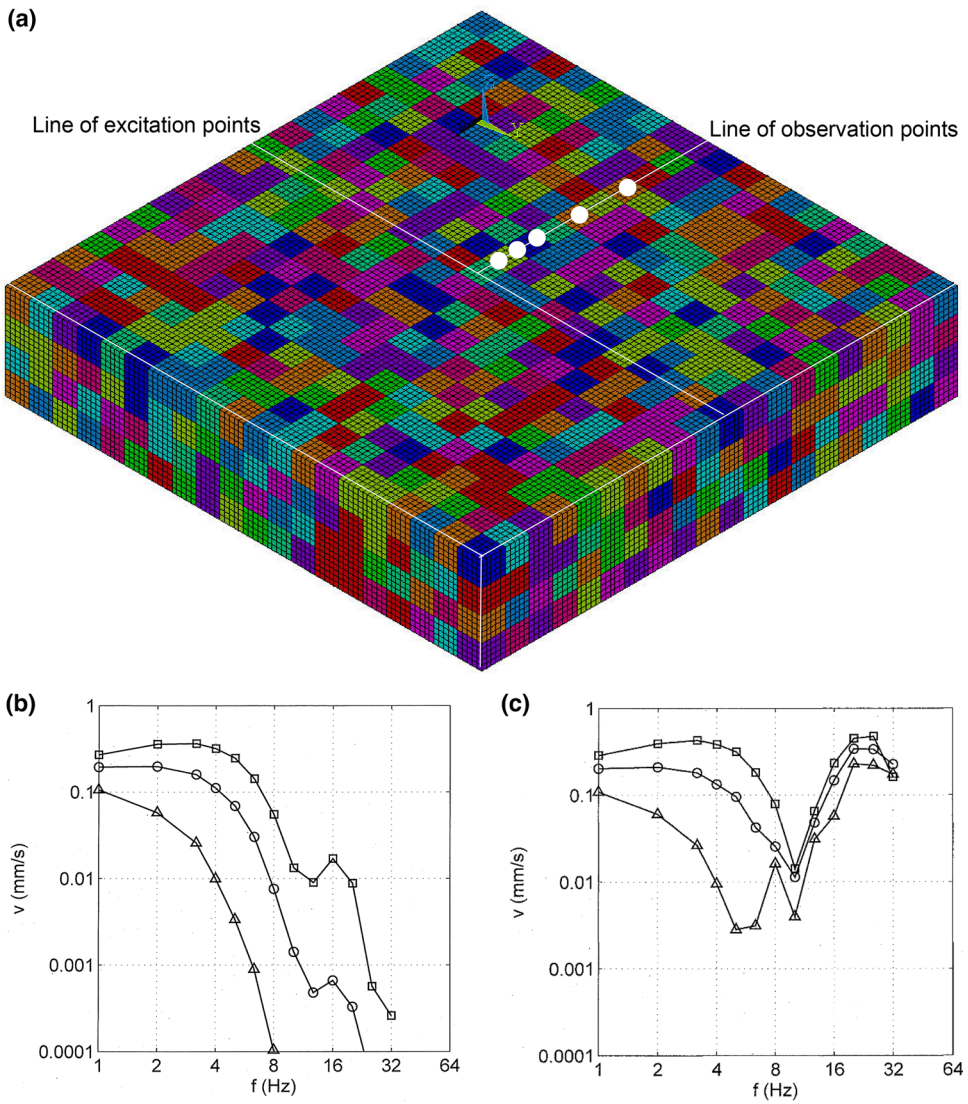

Fig. 11 Low-frequency spectra from the axle pulses on the sleepers in case of a homogeneous soil (**b**) and a randomly inhomogeneous soil (**a**, **c**), at distances $r=$ square 3, circle 5, triangle 10 m

the soil stiffness in Fig. 11a generates a "scattered" component of the quasi-static component at mid frequencies [12, 29] which has a weaker attenuation and dominates the far field of the soil (f = 16–32 Hz in Fig. 11c). The axle impulses from the moving static axle load on different sleepers superpose to result in the regular low-frequency quasi-static response, but in case of a soil with randomly varying stiffness some mid-frequency components of the impulses are left over. This mid-frequency range is clearly speed dependent, it is shifted to higher frequencies for the high speed train in Fig. 8l, n. The scattered axle impulses could be observed at many measurement sites as absolute or relative maxima with only a weak attenuation of the amplitudes.

Conclusion

Hammer- and train-induced ground vibrations have been analysed for 12 sites in Germany and Switzerland. It has been demonstrated that hammer experiments can well be used for the prediction of train vibrations although there are many difference in the type of excitation. The transfer function of a specific site from hammer impact has a strong similarity to the ground vibration spectrum from a train passage. This is due to the fact that the main excitation from railway irregularities has a wide, smooth and regular spectrum which yields also a wide, smooth and regular spectrum of the dynamic axle load. Moreover, this load spectrum is nearly constant at the value 1 kN per axle and one-third octave. Hammer and train spectra are characterised by a low-frequency filter due to the layering and a high-frequency filter due to the material damping of the soil. Therefore, mid-frequencies are always dominating at longer distances. The train-induced ground vibration has a

stronger high-frequency filter because of the load distribution across the track, and a weaker attenuation because of the axle loads distributed along the train. The attenuation with distance has been analysed in detail. The theoretical amplitude-distance law for a homogeneous half-space has been found only for a few sites and for high frequencies. In contrary, the empirical power-law attenuation with frequency-dependent $q(f)$ seems to be appropriate for most of the measured hammer- and train-induced ground vibrations and some reasons have been discussed. The attenuation power q increases with frequency and with hammer excitation (theoretically by $\Delta q = 0.3$ or 0.5), and has been found between 0.6 and 2.5 for hammer and between 0.4 and 2.0 for train excitation at 12 representative sites. The attenuation is site-specific and can be transferred from the hammer impact to the train vibration. The strong attenuation is due to a strong soil damping at the site. For some sites, a very weak attenuation and a clear amplification has been found for a special train-induced mid-frequency component which is attributed to the scattering of the axle impulses due to irregularities on their propagation path.

Acknowledgements Thanks to my colleagues S. Said, W. Schmid, W. Wuttke, and F. Ziegler who helped a lot for the measurements.

Funding Open Access funding enabled and organized by Projekt DEAL. No funds, grants, or other support was received.

Data availability The data are available from the author on request.

Declarations

Conflict of interest The authors have no relevant financial or non-financial interests to disclose.

References

1. Aki K (1957) Space and time spectra of stationary stochastic waves with special reference to microtremors. Bull Earthq Res Inst 35:415–456
2. Alves Costa P (2011) Vibrações do sistema via-maciço induzidas por tráfego ferroviário—modelação numérica e validação experimental. PhD thesis, University of Porto.
3. Arbeitsgemeinschaft Schwingungsausbreitung (1981) Schwingungsausbreitung an Schienenverkehrswegen. Research report, IGI Westheim, LGA Nürnberg, Müller-BBM Planegg
4. Auersch L (1988) Zur Entstehung und Ausbreitung von Schienenverkehrserschütterungen: Theoretische Untersuchungen und Messungen am Hochgeschwindigkeitszug Intercity Experimental. Research report 155, BAM, Berlin
5. Auersch L (1994) Wave propagation in layered soil: theoretical solution in wavenumber domain and experimental results of hammer and railway traffic excitation. J Sound Vib 173:233–264
6. Auersch L (2005) Dynamics of the railway track and the underlying soil: the boundary-element solution, theoretical results and their experimental verification. Veh Syst Dyn 43:671–695
7. Auersch L, Said S (2010) Attenuation of ground vibrations due to different technical sources. Earthq Eng Eng Vib 9:337–344
8. Auersch L (2010) Theoretical and experimental excitation force spectra for railway induced ground vibration—vehicle-track soil interaction, irregularities and soil measurements. Veh Syst Dyn 48:235–261
9. Auersch L (2014) The use and validation of measured, theoretical and approximated point-load solutions for the prediction of train induced vibration in homogeneous and inhomogeneous soils. Int J Acoust Vib 19:52–64
10. Auersch L, Said S (2015) Comparison of different dispersion evaluation methods and a case history with the inversion to a soil model, related admittance functions, and the prediction of train induced ground vibration. J Near Surf Geophys 13:127–142
11. Auersch L (2019) Fast trains and isolating tracks on inhomogeneous soils. In: Krylov V (ed) Ground vibrations from high-speed railways: prediction and mitigation. ICE Publishing, London, pp 27–76
12. Auersch L (2021) Train-induced ground vibration due to the irregularities of the soil. Soil Dyn Earthq Eng 140:106438
13. Auersch L (2023) Wave propagation from hammer, vibrator and railway excitation—theoretical and measured attenuation in space and frequency domain. In: Dimitrovov Z, Biswas P, Gonçalves R, Silva T (eds) Recent trends in wave mechanics and vibrations, WMVC 2022. Mechanisms and machine science 125, pp 352–359
14. Badsar S, Schevenels M, Haegeman W, Degrande G (2010) Determination of the material damping ratio in the soil from SASW tests using the half-power bandwidth method. Geophys J Int 182:1493–1508
15. Bahrekazemi M (2004) Train-induced ground vibration and its prediction. PhD thesis, KTH Stockholm
16. Bayzar M, Song C (2006) Transient analysis of wave propagation in non-homogeneous elastic unbounded domains by using the scaled boundary finite-element method. Earthq Eng Struct Dyn 35:1787–1806
17. Capon J (1969) High resolution frequency-wavenumber analysis. Proc IEEE 57:1408–1418
18. Colombero R, Kontoe S, Foti S, Potts D (2015) Numerical modelling of drop load tests. SDEE 77:279–289
19. Connolly D, Alves Costa P, Kouroussis G, Galvin P, Woodward P, Laghrouche O (2015) Large scale international testing of railway ground vibrations across Europe. Soil Dyn Earthq Eng 71:1–12
20. Degrande G, Schillemanns L (2001) Free field vibrations during the passage of a Thalys high-speed train at variable speed. J Sound Vib 247:131–144
21. El Kacimi A, Woodward P, Laghrouche O, Medero G (2013) Time domain 3D finite element modelling of train-induced vibration at high speed. Comput Struct 118:66–73
22. François S, Schevenels M, Galvín P, Lombaert G, Degrande G (2010) A 2.5D coupled FE-BE methodology for the dynamic interaction between longitudinally invariant structures and a layered halfspace. Comput Methods Appl Mech Eng 199:1536–1548
23. Friedl H, Ralbovsky M, Flesch R (2009) Simulationsverbesserung durch gezielte dynamische in-situ Versuche für Boden und Bauwerk. VDI Berichte 2063. VDI-Verlag, Düsseldorf, pp 133–147

24. Galvin P (2007) Analisis numerico y experimental de las vibraciones ocasionadas por el paso de trenes de alta velocidad en el suelo y en structuras cercana a la via. PhD thesis, University of Sevilla
25. Garburg R, Heiland D, Mistler M (2013) Determination of insertion losses for vibration mitigation measures in track by artificial vibration excitation. In: Proceedings of 11th IWRN, Udevalla, notes on numerical fluid mechanics and multidiscoplinary design 126, pp 237–244
26. Haskell N (1953) The dispersion of surface waves on multilayered media. Bull Seismol Soc Am 43:17–34
27. Haupt W (1988) Ausbreitung von Erschütterungen an Schienenverkehrswegen. In: Steinwachs M (ed) Ausbreitung von Erschütterungen im Boden und Bauwerk. DGEB, Trans Tech Publications, Clausthal, pp 217–229
28. Hölzl G, Fischer G (1985) Körperschall- bzw Erschütterungsausbreitung an oberirdischen Schienenverkehrswegen. Eisenbahntechnische Rundschau 34:469–477
29. Huber G (1988) Erschütterungsausbreitung beim Rad/Schiene-System. PhD thesis, University Karlsruhe
30. Ju S, Lin H (2008) Experimentally investigating finite element accuracy for ground vibrations induced by high-speed trains. Eng Struct 30:733–746
31. Kausel E, Roesset J (1981) Stiffness matrices for layered soils. Bull Seismol Soc Am 71:1743–1761
32. Kim D, Lee J (2000) Propagation and attenuation characteristics of various ground vibrations. Soil Dyn Earthq Eng 19:115–126
33. Lamb H (1904) On the propagation of tremors over the surface of an elastic solid. Philos Trans R Soc Lond A203:1–42
34. Lombaert G, Degrande G (2009) Ground-borne vibration due to static and dynamic axle loads of InterCity and high-speed trains. J Sound Vib 319:1036–1066
35. Lombaert G, Ekblad A, Cuéllar V et al (2013) Mitigation measures on the transmission path: results of field tests. RIVAS Deliverable D4.5, International Union of Railways, Paris
36. Maldonado M (2008) Vibrations dues au Passage d'un Tramway: Mesures Experimentales et Simulations Numériques. PhD thèse, Ecole Centrale de Nantes.
37. Mistler M, Heiland D (2009) Erschütterungsprognosen mit Hilfe künstlicher Anregungsmethoden. VDI Berichte 2063. VDI Verlag, Düsseldorf, pp 13–28
38. Mussat J, Bertero R, Barbieri P (2019) Propagation and attenuation of statistically stationary ground vibrations due to human activities. GGE 145:1–43
39. Nazarian S (1984) In situ determination of elastic moduli of soil deposits and pavement systems by spectral-analysis-of-surface-waves method. PhD thesis, University of Texas, Austin
40. Nelson J, Saurenman H (1987) A prediction procedure for rail transportation groundbourne noise and vibration. Transp Res Rec 1143:26–35
41. Park C, Miller R, Xia J (1999) Multichannel analysis of surface waves. Geophysics 64:800–808
42. Romero A (2012) Predicción, medida experimental y evaluación de las vibraciones producidas por el tráfico ferroviario. PhD thesis, University of Sevilla
43. Sato H, Fehler M (1998) Seismic Wave Propagation and Scattering in the Heterogeneous Earth. Springer and American Institute of Physics, New York
44. Saurenman H (1996) High speed rail ground-borne vibration test results. APTA Track, Noise & Vibration Meeting, Portland
45. Steinhauser P (1994) VibroScan—a special seismic method for environmental vibration protection projects. In: Tagungsband 56th EAEG meeting, Wien, pp 1052–1053
46. Takemiya H (2001) Ground vibrations alongside tracks induced by high-speed trains: prediction and mitigation. In: Krylov V (ed) Noise and vibration from high-speed trains. Thomas Telford, London, pp 347–381
47. Thomson W (1950) Transmission of elastic waves through a stratified solid medium. J Appl Phys 21:89–93
48. Triepaischajonsak N, Thompson D, Jones C, Ryue J, Priest J (2011) Ground vibration from trains: experimental parameter characterisation and validation of a numerical model. Rail Rapid Transit 225:140–153
49. Wolf J (1985) Dynamic soil-structure interaction. Prentice-Hall, Englewood Cliffs
50. Yang Y, Hung H, Chang D (2003) Train induced wave propagation in layered soils using finite/infinite element simulation. SDEE 23:263–278